Predicting Tropical Cyclogenesis with a Global Mesoscale Model: Hierarchical Multiscale Interactions During the Formation of Tropical Cyclone Nargis (2008)

B.-W. Shen,W.-K. Tao, W. K. Lau , R. Atlas

Popular Summary

In this article, the formation of TC Nargis is studied with the global mesoscale model to address the following questions: (1) to what extent can large-scale flows determine the timing and location of TC genesis and (2) if and how realistically can a high-resolution global model depict those processes. TC Nargis devastated Myanmar in the Indian Ocean in early May 2008, caused over 133,000 fatalities and $10 billion in damage, and became one of the 10 deadliest tropical cyclones (TCs) of all time.

It is found that the initial formation and intensity variations of TC Nargis can be realistically predicted up to 5 days in advance. Preliminary analysis suggests that improved representations of the following environmental conditions and their hierarchical multiscale interactions were the key to achieving this lead time: (1) a westerly wind burst and equatorial trough, (2) an enhanced monsoon circulation with a zero wind shear line, (3) good upper-level outflow with anti-cyclonic wind shear between 200 and 850 hPa, and (4) low-level moisture convergence.

JOURNAL OF GEOPHYSICAL RESEARCH, VOL. 115, D14102, doi:10.1029/2009JD013140, 2010

Predicting tropical cyclogenesis with a global mesoscale model: Hierarchical multiscale interactions during the formation of tropical cyclone Nargis (2008)

B.-W. Shen,[1,2] W.-K. Tao,[1] W. K. Lau,[1] and R. Atlas[3]

Received 3 September 2009; revised 1 February 2010; accepted 19 March 2010; published 17 July 2010.

[1] Very severe cyclonic storm Nargis devastated Burma (Myanmar) in May 2008, caused tremendous damage and numerous fatalities, and became one of the 10 deadliest tropical cyclones (TCs) of all time. To increase the warning time in order to save lives and reduce economic damage, it is important to extend the lead time in the prediction of TCs like Nargis. As recent advances in high-resolution global models and supercomputing technology have shown the potential for improving TC track and intensity forecasts, the ability of a global mesoscale model to predict TC genesis in the Indian Ocean is examined in this study with the aim of improving simulations of TC climate. High-resolution global simulations with real data show that the initial formation and intensity variations of TC Nargis can be realistically predicted up to 5 days in advance. Preliminary analysis suggests that improved representations of the following environmental conditions and their hierarchical multiscale interactions were the key to achieving this lead time: (1) a westerly wind burst and equatorial trough, (2) an enhanced monsoon circulation with a zero wind shear line, (3) good upper-level outflow with anti-cyclonic wind shear between 200 and 850 hPa, and (4) low-level moisture convergence.

Citation: Shen, B.-W., W.-K. Tao, W. K. Lau, and R. Atlas (2010), Predicting tropical cyclogenesis with a global mesoscale model: Hierarchical multiscale interactions during the formation of tropical cyclone Nargis (2008), *J. Geophys. Res.*, *115*, D14102, doi:10.1029/2009JD013140.

1. Introduction

[2] Each year tropical cyclones (TCs) cause tremendous economic losses and many fatalities throughout the world. For example, Katrina (2005), the costliest Atlantic hurricane in history, caused severe destruction in New Orleans and the surrounding Gulf Coast region and was responsible for about $80 billion in damage. Recently, TC Nargis devastated Myanmar in the Indian Ocean in early May 2008, causing over 133,000 fatalities and $10 billion in damage. In response to this tragedy, more than 40 countries sent relief to Myanmar, showing the broad range of its impact. To reduce these losses, it is crucial that the lead time for the accurate prediction of TC formation, intensification, and movement is extended. However, although TC track forecasts have steadily improved over the past decades, progress on short-term intensity and formation forecasts has been very slow. A major challenge in the prediction of TC genesis is, among other things, the accurate simulation of complex interactions across a wide range of scales, from the large-scale environment (deterministic), to mesoscale flows, down to convective-scale motions (stochastic).

[3] Historically, numerical modeling has been a very powerful way to hypothesize and test the physical mechanisms associated with TC formation and intensification. Our current level of understandings on this topic suggests that the following processes may be involved: (i) large-scale processes such as baroclinic/barotropic instability, tropical easterly waves, the Madden-Julian Oscillation (MJO) [*Madden and Julian*, 1971; *Maloney and Hartmann*, 2000a, 2000b] and monsoons, (ii) mesoscale processes such as vortex mergers and vortex axisymmetrization [*Hendrick et al.*, 2004; *Montgomery et al.*, 2006; *Ritchie and Holland*, 1997; *Simpson et al.*, 1997] and (iii) small-scale processes such as latent heat release by deep convection (e.g., conditional instability of the second kind or CISK) [*Charney and Eliassen*, 1964; *Ooyama*, 1964] and surface heat and moisture fluxes from the ocean (e.g., wind induced surface heat exchange or WISHE) [*Emanuel*, 1986]. A review is given by *Dunkerton et al.* [2008]. Processes from the above three categories have been shown to be applicable at different stages of a TC's life cycle, including the early, the transient, and the deepening stage.

[4] As smaller-scale (convective) processes (associated with a vortex) could be modulated and/or constrained by larger-scale deterministic processes [e.g., *Simpson et al.*,

[1]Laboratory for Atmospheres, NASA Goddard Space Flight Center, Greenbelt, Maryland, USA.
[2]ESSIC, University of Maryland, College Park, Maryland, USA.
[3]AOML, NOAA, Miami, Florida, USA.

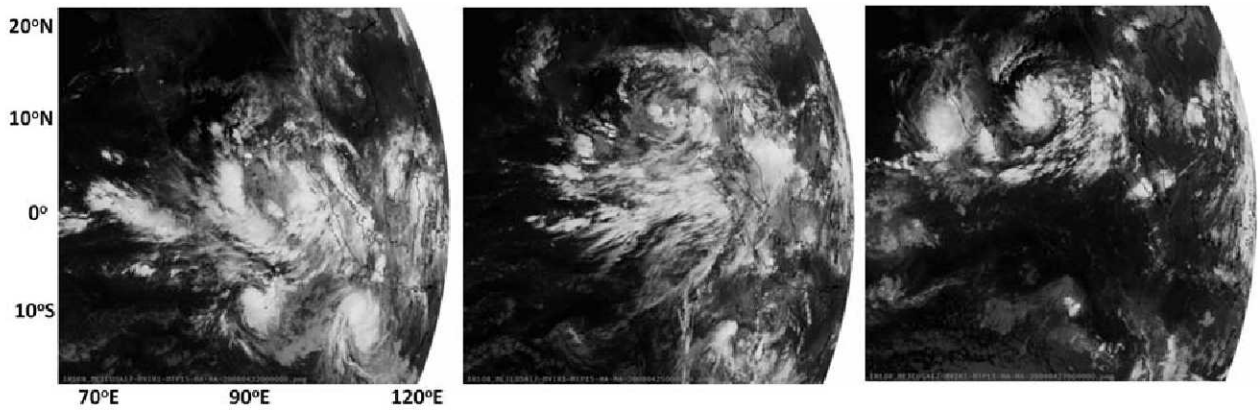

Figure 1. METEOSAT 7 IR images over the Indian Ocean in late April 2008: (left) tropical cyclones Durga and Rosie south of a westerly wind burst/jet (WWB) at 0000 UTC 22 April, (middle) a pre-TC disturbance that appeared north of the WWB at 0000 UTC 25 April, and (right) the formation of TC Nargis at 1200 UTC 27 April.

1997], an improved ability to simulate the latter might help increase the accuracy of simulating the former. Therefore, with the short-term goal of extending the lead time of TC prediction, the main focus will be the model's ability to simulate multiple processes and multiscale interactions during the early and transient stages related to TC formation. This is also important for understanding model performance in simulating climate and the impact of climate change on long-term TC variations. It has been widely accepted that the following six climatological (environmental) conditions are important for TC formation: warm sea surface temperatures (SSTs), high relative humidity, conditional instability, high low-level relative vorticity, weak vertical shear, and being displaced away from the equator (e.g., beyond 5° in latitude). During the past several decades, it has been shown that TC genesis statistics at long time scales (e.g., seasonal) are closely related to these conditions [e.g., *Gray*, 1975, 1979]. However, to improve TC forecasts at shorter time (i.e., 5 to 10 day) and smaller spatial scales, additional details are still needed. For example, environmental factors favorable for TC formation in the Indian Ocean include an enhanced monsoon circulation and anti-cyclonic shear between 200 and 850 hPa [e.g., *McBride and Zehr*, 1981] (see section 3 for a more detailed discussion). Favored locations for TC formation include north (south) of the monsoon equatorial trough in the Northern (Southern) Hemisphere where cyclonic shear exists. In addition, previous studies with idealized models suggested that large-scale organized convective systems accompanying the MJO [*Madden and Julian*, 1971] might regulate the genesis of twin TCs [e.g., *Ferreira and Schubert*, 1996]. More recent studies have suggested that induced equatorial Rossby waves and westerly wind bursts (WWBs) could be a precursor to the genesis of twin TCs [*Aiyyer and Molinari*, 2003] and that wave accumulation due to scale contraction [e.g., *Webster and Chang*, 1988] could provide a downscale energy and vorticity transfer that leads to TC formation [*Holland and Webster*, 2005; *Kuo et al.*, 2001].

[5] The aforementioned studies collectively suggest that extending the warning time for TC genesis in the Indian Ocean would require a numerical model that could better simulate the multiscale environmental flow and its modulation on TC activity. This goal might be achieved by recent advances in high-resolution global models and supercomputing. As these models have shown the potential to improve TC track and intensity forecasts [*Atlas et al.*, 2005, 2007; *Shen et al.*, 2006a, 2006b], their ability to depict the processes that contribute to the formation of TCs in the Indian Ocean is being examined (e.g., twin TCs in work by *Shen et al.* [2007]). In this study, simulations of TC Nargis will be analyzed because its short life cycle and unusual recurvature make it a challenge to predict. The Nargis case as well as others are being studied to address the following questions: (1) to what extent can large-scale flows determine the timing and location of TC genesis (e.g., Nargis in this study) and (2) if and how realistically can a high-resolution global model depict those processes. While a general predictability problem would require a "perfect" numerical model and "perfect" initial state, only the predictive capabilities of one specific high-resolution global model will be studied to "illustrate" the potential predictability of a TC. The numerical approach is described in section 2, and the results are discussed in section 3. Concluding remarks are given at the end.

2. Numerical Approach

[6] Satellite METEOSAT 7 IR images over the Indian Ocean (Figure 1) show that TCs Durga and Roise first appeared in the Southern Hemisphere (SH) in late April 2008. Five days later on April 27th, TC Nargis formed in the Northern Hemisphere (NH). During this seasonal transition period, a WWB (and an equatorial trough) associated with a monsoon-like circulation and/or a weak MJO moved northward from the SH to the NH. The latitudinal variation and movement of the WWB and MJO might have lead to the formation of the aforementioned TCs, which appeared, following a time lag, asymmetrically in space and time with respect to the equator. Therefore, an accurate prediction of the northward movement of the WWB would be crucial for extending the lead time for TC Nargis. In contrast, for the prediction of the twin TCs, which appear in association with an MJO that is symmetric with respect to the equator, it is

Table 1. Numerical Experiments With Different Modeling Configurations[a]

Case ID	IC	RES	Grid-Scale Condensation	CPS	Relaxation Time (hours)	5° Ave Precip (mm/d)	2° Ave Precip (mm/d)	Max 10m Wind Speed (m/s)
CNTL	04/22	0.25^o	x		-	59.7	152.2	30
E-23	04/23	0.25^o	x		-	63.7	192.1	33
E-24	04/24	0.25^o	x		-	59.5	172.9	30
D-E	04/22	0.5^o	x		-	n/a	n/a	n/a
D-CPS	04/22	0.5^o	x	x	3	44.0	114.6	20
D-CPS6h	04/22	0.5^o	x	x	6	64.0	128.1	27

[a]Case ID is the case name; IC is the starting date of initial condition. RES is the model resolution; Grid-Scale and CPS indicate the usage of an explicit grid-scale condensation scheme or cumulus parameterizations; Relaxation denotes the relaxation time in the CPs; 5° Ave and 2° Ave show the temporal and spatial averaged precipitation during the period April 27–29 in a 5° (2°) box centered at the precipitation maximum near the vortex center. Max 10m is the maximum 10m wind speed near the eye of the simulated Nargis at 1200 UTC April 28 2008. The corresponding TRMM precipitation is 61.8 (173.8) mm/day in a 5° (2°) box, and QuikSCAT wind speed is 27 m/s. The best track gave a max sustained wind speed of 33.4 m/s (65 knots) at this time.

important to accurately simulate the eastward propagation of the WWB [*Moncrieff et al.*, 2007; *Shen et al.*, 2007].

[7] Cyclone Nargis, which devastated Burma (Myanmar) in early May 2008, is one of the 10 deadliest TCs in recorded history. According to the Joint Typhoon Warning Center (JTWC, http://weather.unisys.com/hurricane/archive/08042706, 2008), Nargis was first identified as a tropical system at 1200 UTC 27 April 2008 in the central Bay of Bengal near latitude 12.1°N and longitude 85.6°E. In comparison, a depression was identified 9 hours earlier by the India Meteorological Division (IMD) at 0300 UTC April 27 near latitude 12°N and longitude 87.0°E. Initially, Nargis moved slowly in a northwest direction. Under the influence of both a sub-tropical ridge to the northwest and a near-equatorial ridge to the southeast, Nargis gradually recurved, turning northward at 1800 UTC April 28th, and northeastward at 0600 UTC April 29th. Nargis began moving nearly eastward at 1200 UTC May 1st, which is very unusual movement for TCs in this basin, and intensified into a Category 4 storm on May 2nd. At its strongest intensity, it was estimated to have a minimum sea-level pressure (MSLP) of 960 hPa and peak winds of 135 mph. It made landfall in the Ayeyarwady division of Burma (Myanmar) at 1200 UTC May 2nd before passing close to the highly-populated capital city of Yangon. It then dissipated near the Myanmar-Thailand border. Thirty-seven townships with a population of 2.4 million were affected by TC Nargis. As of 16 May 2008, the official number of dead and missing people was over 133,000 (OCHA report, Myanmar: Cyclone Nargis, 2008, http://ochaonline.un.org/MyanmarSituationReports/tabid/4600/Default.aspx). The storm's formation, recurvature and especially its rapid intensification, which involved multiscale interactions such as the influence of both the sub-tropical and near-equatorial ridges, made it a real challenge to predict in advance.

[8] In this study, a global mesoscale model (GMM) [e.g., *Shen et al.*, 2006a] deployed on the NASA Columbia supercomputer [*Biswas et al.*, 2007] is used to conduct numerical experiments. The GMM, previously called the high-resolution finite-volume GCM (fvGCM), has three main components: (1) finite-volume dynamics [*Lin*, 2004], (2) NCAR CCM3 physics, and (3) the NCAR Community Land model. In the model, the *Zhang and McFarlane* [1995] and *Hack* [1994] schemes are used for deep convection and shallow-to-midlevel convection, respectively. After these cumulus parameterizations (CPs) are called, a large-scale condensation scheme [*Sundqvist*, 1988] is applied. Without these CPs, latent heat release comes from the grid-scale condensation processes. Dynamic initial conditions (ICs) and sea surface temperature (SST) are derived from GFS T384 analysis data and 1° optimum interpolation SSTs from the National Centers for Environmental Prediction (NCEP). No vortex initialization (e.g., bogusing) scheme is applied to the initial fields. Our previous studies with more than sixty 5-day runs have shown that the model with 1/8 degree of horizontal resolution and disabled CPs was able to produce remarkable forecasts of track and intensity associated with intense Atlantic hurricanes in 2004 and 2005. Realistic TC vertical structures (e.g., Katrina) were also simulated, including maximum horizontal winds near the top of the boundary layer, a narrow eyewall, and an elevated warm core [e.g., *Shen et al.*, 2006a, 2006b].

[9] NCEP weekly Reynolds SSTs are used during the integration and show relatively high values (28°–30°C) in the North Indian Ocean Basin during this period. Simulation results for TC Nargis will be discussed with a focus on genesis processes. NASA QuikSCAT [*Liu et al.*, 1998] and TRMM satellite data and NCEP GFS analyses will be used for model validation. For simplicity, genesis is defined as the formation of a low-level closed circulation having a minimum sea-level pressure (MSLP) below 1000 hPa, an elevated warm core and a tendency for further intensification. TC best tracks are from the JTWC (http://weather.unisys.com/hurricane/archive/08042706, 2008), unless otherwise stated. (Because the time difference between a tropical depression and a self-sustaining vortex might be 12–24 hours [*Briegel and Frank*, 1997], we don't make an attempt at determining the exact time of genesis.) Three 7-day simulations initialized at 0000 UTC April 22–24 are conducted at a 1/4 degree resolution with an explicit grid-scale condensation scheme [*Sundqvist*, 1988]. This model configuration provides consistent simulations of TC genesis and is computationally more advantageous than using higher resolutions; therefore, it is more feasible for hurricane climate studies in the near future. Three additional experiments at a coarser (0.5°) resolution are performed with and without CPs for comparison. These six experiments are briefly summarized in Table 1.

3. Numerical Results

3.1. Control Experiment

[10] Three consecutive 7-day 0.25° forecasts initialized at 0000 UTC April 22–24 were performed, which are labeled as CNTL, E-23, and E24, respectively. The control run was

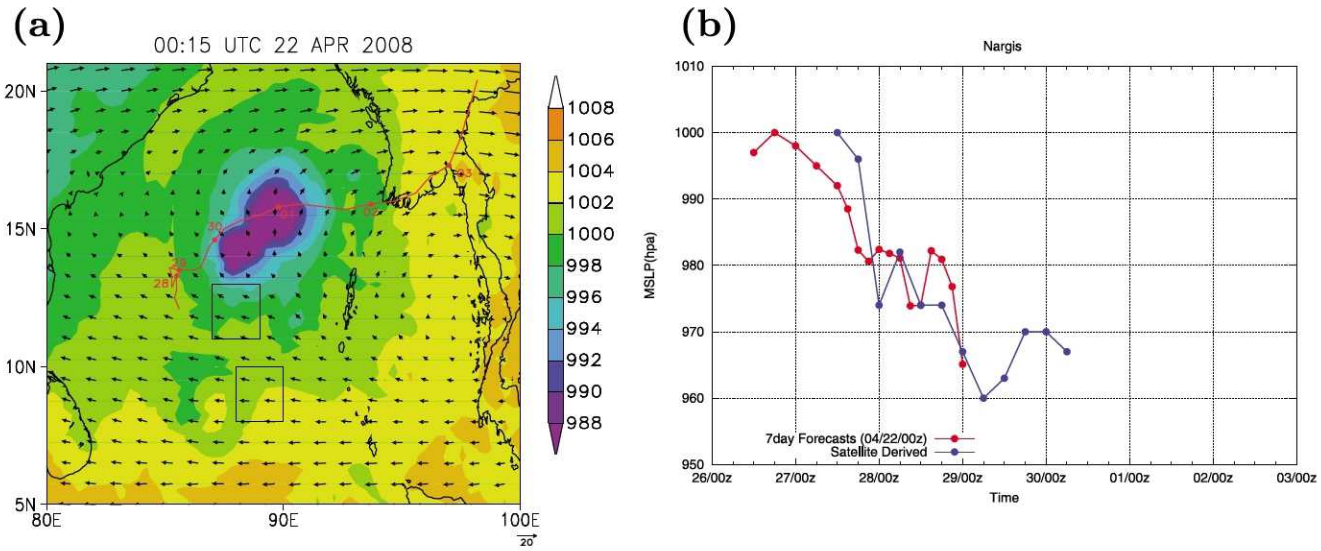

Figure 2. Seven-day forecast of sea level pressure (SLP) starting at 0000 UTC 22 April, 2008. (a) Spatial distribution of minimum SLP over the period (shaded) and average 200-hPa winds (vector), qualitatively showing the initial location and subsequent movement of Nargis in the model. Two square boxes indicate the location of a pre-TC disturbance. The average 850-hPa wind convergences over each box is shown in Figure 5. (b) Temporal evolution of minimal SLP of Nargis in the model from day 5 to day 7 of integration (red), and the corresponding minimal SLP derived from satellite data (blue). It should be noted that TC Nargis made landfall 1200 UTC 2 May.

initialized 132 (123) hours prior to the first record of TC Nargis by JTWC (IMD). The other two runs were initialized at different times to verify the model's consistency in simulating the formation of Nargis and will be briefly discussed near the end of this section. In the CNTL case, the spatial distribution of MSLP over this period (Figure 2a) roughly shows the initial formation and subsequent movement of the model TC. Figure 2b shows the intensity change of the TC in the model after its formation from 108 to 144 h into the integration. Both the track and intensity forecasts are in good agreement with the best track, but the predicted propagation speed is faster. The simulated TC first forms after 108 h of simulation at 1200 UTC April 26th, which is about 24 (15) hours earlier than the observed TC by JTWC (IMD). The 850 hPa winds for the model TC and its surrounding environmental flows after 126 h of simulation are shown in Figure 3a and the corresponding NCEP analysis in Figure 3b. In the Bay of Bengal, a WWB appears at low latitudes (0–10°N) while sub-tropical westerly winds appear along 20°N near the Himalayas. The model simulation clearly shows a pair of Rossby gyres (e.g., along longitude 90°E). Overall, the NCEP analysis shows a similar pattern (Figure 3b) but does not resolve Nargis very well during the period 22–29 April due to the sparsity of observations in this region. It is likely that TC Nargis could be influenced by these surrounding environmental flows, including the location and strength of the WWB and the flows deflected by the Himalayan mountains. Though there exists a pair of equatorial Rossby waves in the low levels (Figure 3), which are asymmetric with respect to the equator, no TC formed in the southern hemisphere. This is partly because of the increased vertical wind shear associated with the movement of easterly winds on top of the low-level cyclonic circulation (not shown).

[11] In Figure 4, the northward movement of the WWB in the numerical simulations is verified against NCEP analysis. Figures 4a–4c show time-longitude cross sections of the NCEP 850 hPa zonal winds averaged from 5°S to the equator, from the equator to 5°N, and from 5°N to 10°N, respectively. The corresponding simulated zonal winds are shown in Figures 4d–4f. Overall, the average zonal winds from the 7-day simulations are in good agreement with the NCEP analysis. At low levels (e.g., 850 hPa), the WWB is clearly identified along longitude 90°E, while an easterly wind maximum is evident along longitude 180°E (Figure 4c). At upper levels (e.g., 200 hPa), the wind pattern is nearly reversed with easterly and westerly wind maxima along longitudes 90°E and 150°W (not shown), respectively. The (low-level) WWB between 5°S and 0° starts to weaken around April 25th, because the winds along its leading edge in the SH are deflected southward and the WWB moved northward with the equatorial trough. The latter is indicated by the occurrence of the WWB at higher latitudes (Figures 4b and 4c). The 200 hPa easterly winds in this area show similar intensity variations related to this northward movement (not shown).

[12] Figures 5a and 5b show latitude-time profiles of simulated zonal winds along 89E° and 88E°, respectively; they clearly show that the WWB moves northward with time. During the period of 1200 UTC April 24th to 0000 UTC April 25th, the leading edge of the westerly winds has a "burst", jumping northward to latitude 9°N where easterly winds re-appear several hours later but last for less than 12 hours. The occurrence of horizontal cyclonic wind shear is tied to the formation of a disorganized mesoscale vortex (referred to as a pre-TC disturbance, Figure 6a). In comparison, Figure 5c shows 850 hPa wind convergence averaged over a 2° × 2° box centered at (9°N, 89°E) in red and at

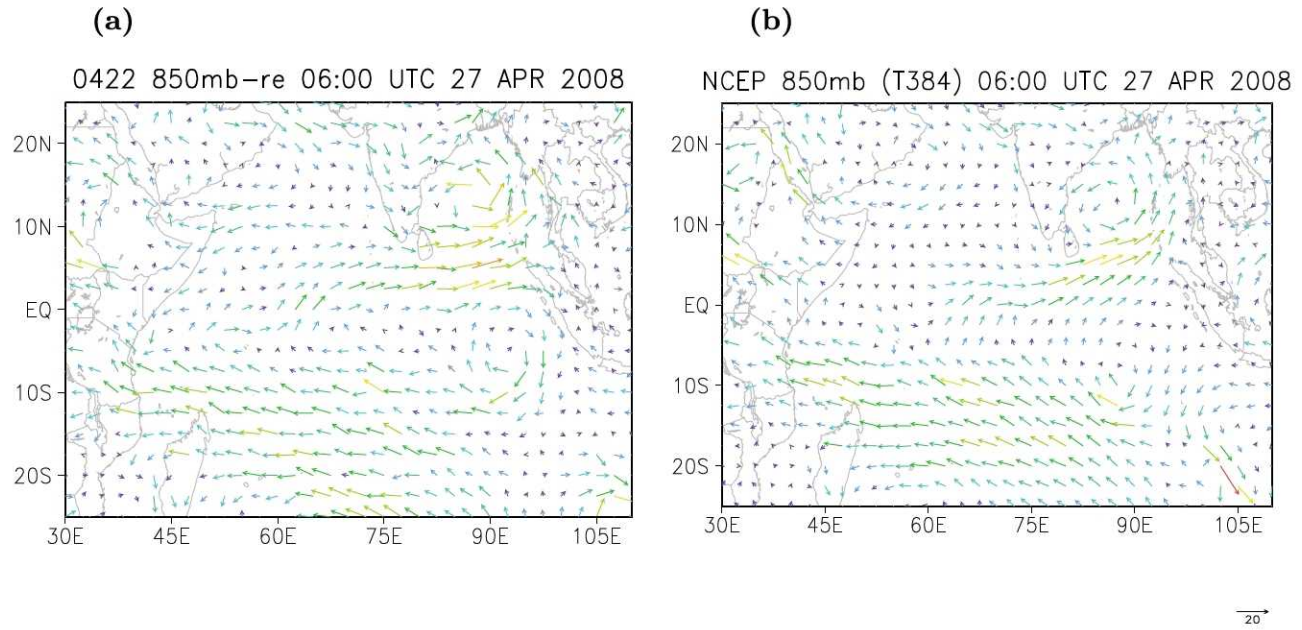

Figure 3. Snapshot of the (a) 850-hPa winds after 126 h of simulation and (b) NCEP analysis at this time (0600 UTC 27 Apr 2008). Both are regridded to a 2.5° × 2.5° resolution. The model simulation clearly shows a pair of Rossby gyres (e.g., along longitude 90°E). During the period 22–29 April, TC Nargis is not well analyzed in the NCEP analysis due to the sparsity of observations in this region.

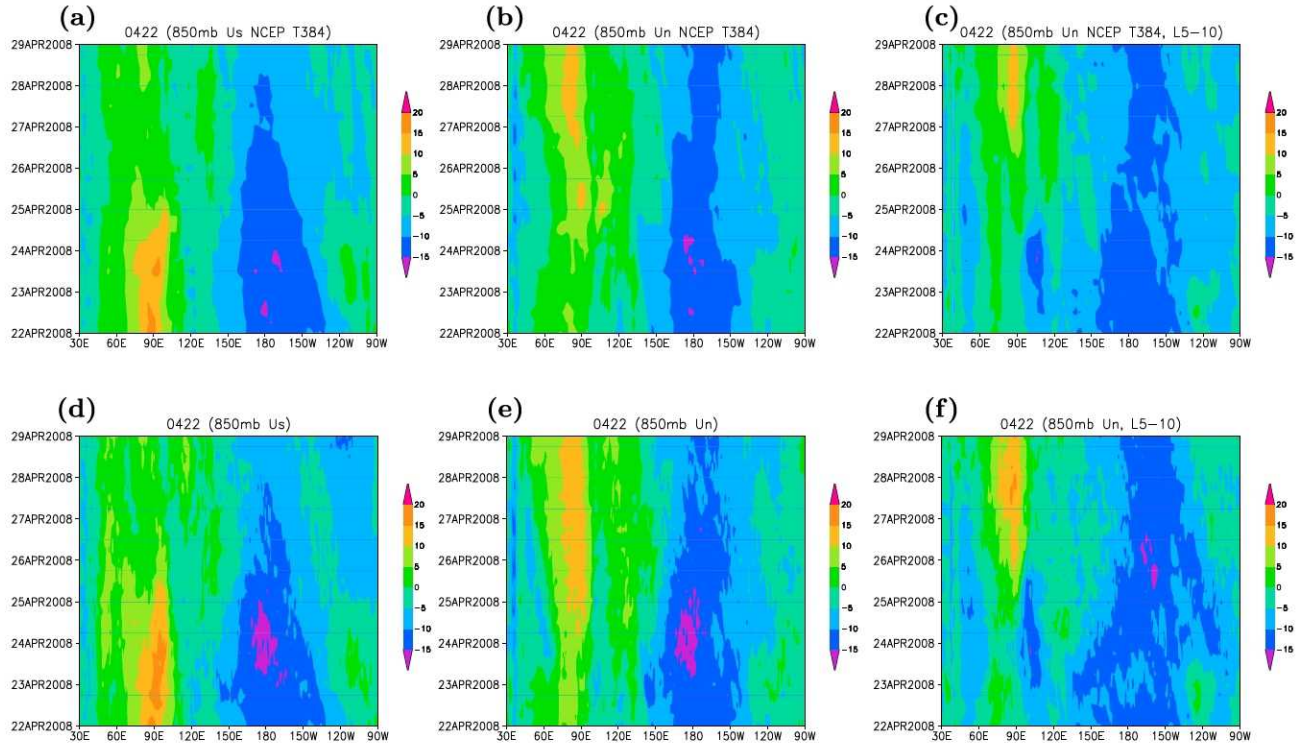

Figure 4. Northward movement of the westerly wind burst shown in time-longitude diagrams of average 850-hPa zonal winds, averaged over (a, d) (5°S, 0°), (b, e) (0°, 5°N), and (c, f) (5°N, 10°N). Figures 4a–4c are for NCEP analysis data during April 22–29, 2008. Figures 4d–4f are for a 7-day model simulation initialized at 0000 UTC April 22, 2008.

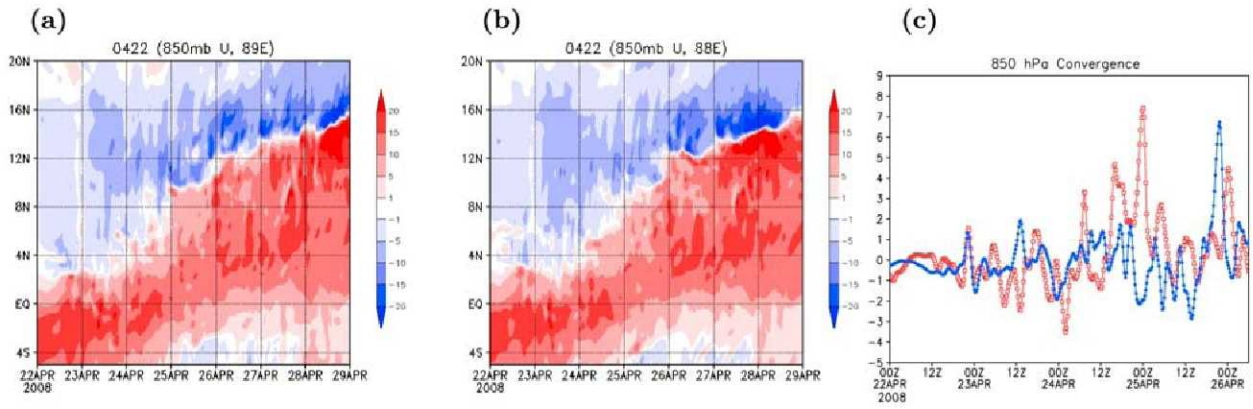

Figure 5. Northward movement of the westerly wind burst shown in latitude-time diagrams of 850 hPa zonal winds along longitudes (a) 89E° and (b) 88E°. (c) The 850 hPa wind convergence (units: $10^{-5}s^{-1}$) averaged over a 2° × 2° box centered at (9°N, 89°E) in red and at (12°N, 88°E) in blue.

(12°N, 88°E) in blue (indicated by the two small boxes in Figure 2). Within the first 2° × 2° box, there exists a peak in low-level convergence during this period (shown by the red line in Figure 5c), suggesting it may have had an important role in the formation of the pre-TC disturbance. Along longitude 88°E, there is another "burst" of westerly winds to 12°N at around 0000 UTC 26 April, which is consistent with the appearance of strong 850 hPa wind convergence (shown by the blue line in Figure 5c). Moreover, the mesoscale vortex becomes more organized at this time (Figure 6b). Over the next 24 hours, the pre-TC disturbance intensifies as revealed in animations of relative vorticity and total precipitable water, which show axisymmetrization of a weak mesoscale vortex. Afterward, a model TC forms with a MSLP of less than 1000 hPa. While the initial propagation and/or intensification of the pre-TC disturbance (or the TC) might be a response to the northward movement of the equatorial trough, the enhanced local circulation (i.e., southwesterly winds) associated with the intensifying vortex could also contribute to the WWB strength at later times. For example, in Figure 3, the simulation of the WWB with a more realistic mesoscale vortex is stronger than the one resolved in the NCEP analysis. To validate the model performance in simulating the timing and location of the pre-TC mesoscale vortex, NASA QuikSCAT surface winds from 0000 UTC April 24 to 1200 UTC April 29 are shown in Figure 7. Overall, the location of the simulated mesoscale vortex is in good agreement with QuikSCAT, but the timing of its formation is several hours (but less than 12 hours) too early. To determine the exact time lag would require higher temporal resolution observations.

[13] Observations have shown that the local monsoon circulation is an important factor in modulating the formation of TCs in this region. Figure 8 shows a time series of height-latitude cross sections of simulated zonal winds (averaged over longitudes 80–90°E) at 1200 UTC April 23, 25, and 27, and height-longitude cross sections of meridional winds (averaged over latitudes 9–16°N) at 1200 UTC April 25, 26, and 27. While the low-level WWB moved northward from the equator, the low-level easterlies north of the WWB also moved slowly northward in the direction of the Himalayas, where they could be partly blocked (Figure 8a). In comparison, southerly (northerly) winds appear to the east (west) of the trough (Figure 8d). Figures 8a

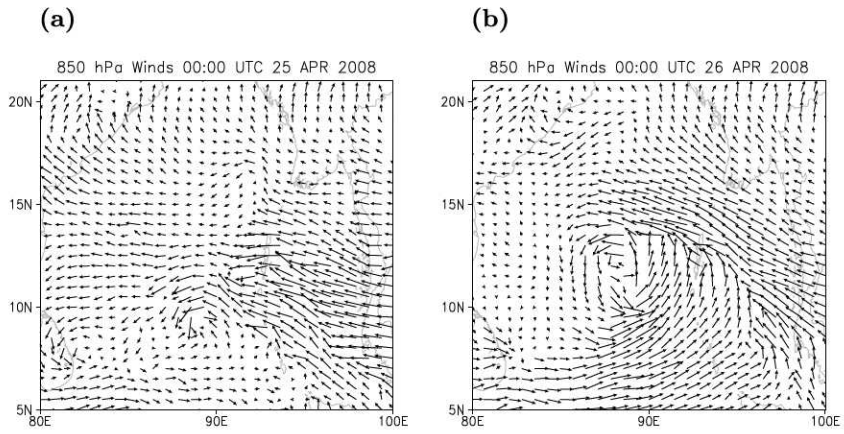

Figure 6. Low-level (850 hPa) winds at 0000 UTC April (a) 25 and (b) 26 after 72 and 96 h of simulation, respectively. A pre-TC disturbance (mesoscale vortex) is first simulated at 0000 UTC April 25, as compared to the QuikSCAT sea surface winds (Figure 7d).

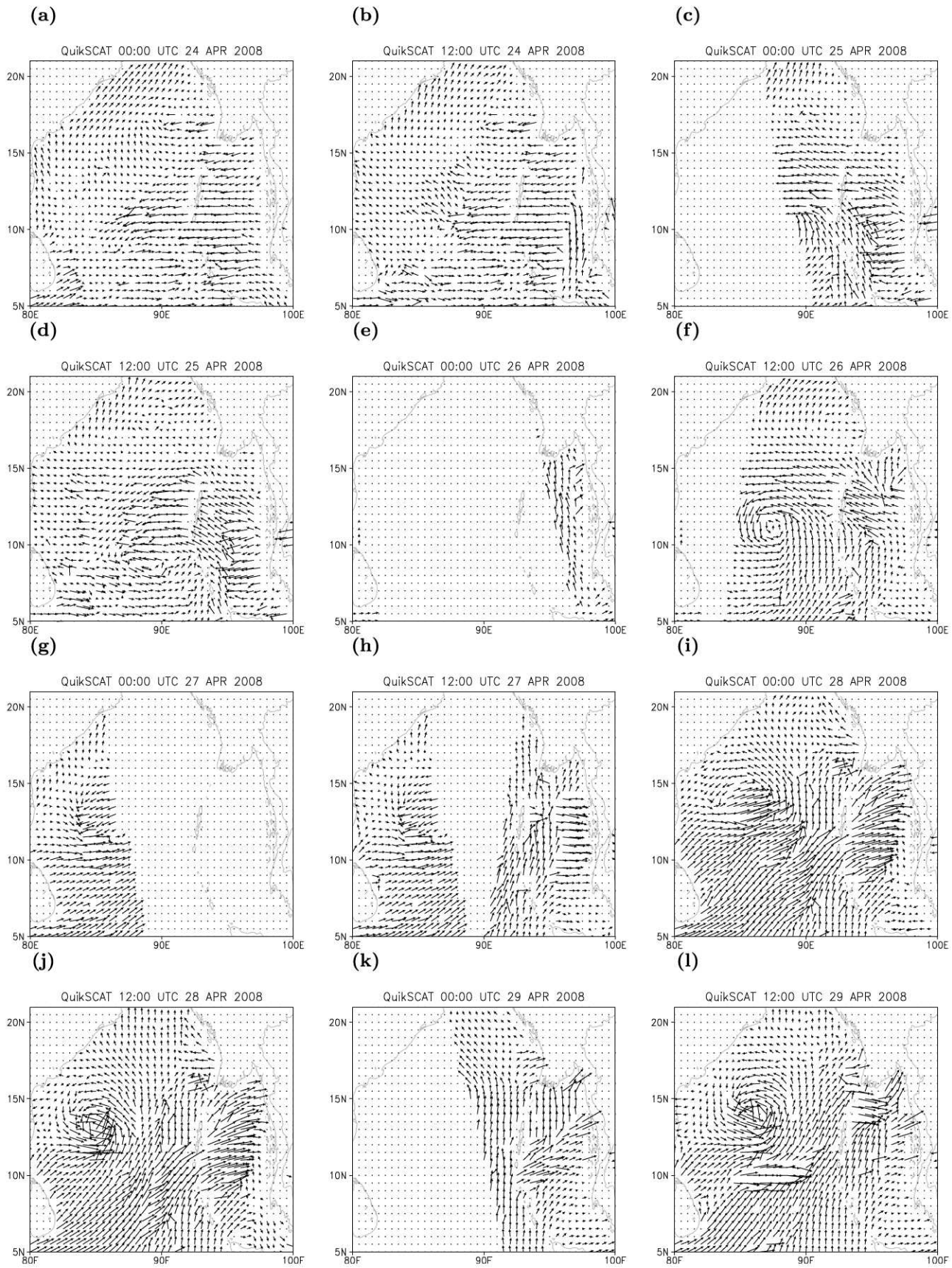

Figure 7. NASA QuikSCAT 0.25° sea surface winds at 0000 and 1200 UTC between 25 and 29 April 2008. Data source: ftp://podaac.jpl.nasa.gov/pub/ocean_wind/quikscat/L3/data/2008/.

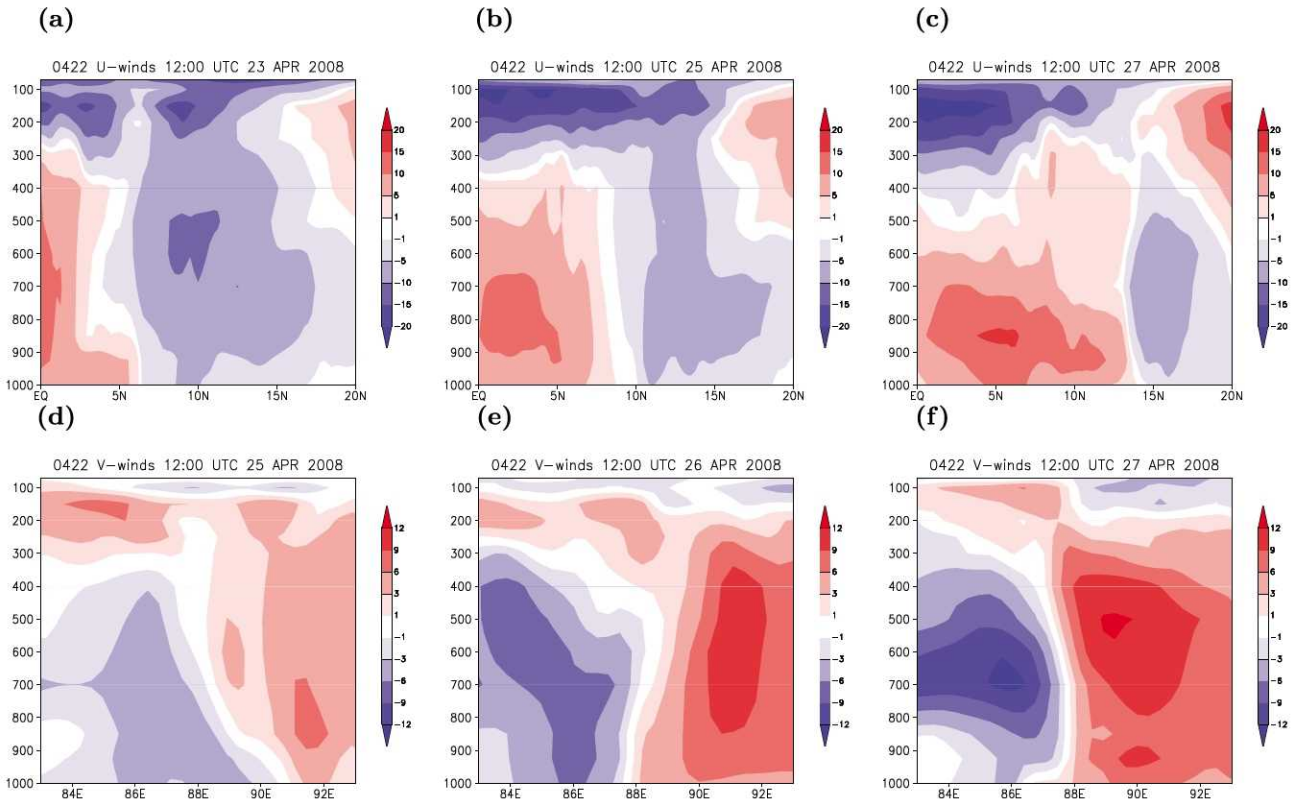

Figure 8. Time evolution of the lateral monsoon circulation and equatorial trough. (a–c) Altitude-latitude cross sections of zonal winds averaged over longitude 80°E to 90°E at 1200 UTC 23, 25, and 27 April 2008, respectively. (d–f) Altitude-longitude cross sections of meridional winds averaged over latitude 9°N and 16°N at 1200 UTC 25, 26, and 27 April 2008, respectively.

and 8d suggest there is a large-scale cyclonic circulation (CC) in the low- and middle-levels (from the surface up to 400 hPa) and a large-scale anti-cyclonic circulation (AC) in the upper-levels. As the equatorial trough, indicated by the zero-wind speed line, moved with the WWB, the orientation of the isotachs in the height-latitude cross sections becomes vertical at low levels. The corresponding zero wind shear line inside this enhanced monsoon circulation is a favored location for TC genesis as suggested by *McBride and Zehr* [1981]. The formation of Nargis in the model appears at 1200 UTC April 26 as the wind-reversal line (trough) approaches latitude 12.5°N. By 1200 UTC April 27, the low- and middle-level CC becomes superimposed with the approaching upper-level AC, providing an ideal outflow (Figure 8c) for further TC intensification (Figure 2b).

[14] A time series of the vertical shear between 200 and 850 hPa is plotted in Figure 9. Anti-cyclonic wind shear is clearly apparent at 0600 UTC April 26 and 27. The anti-cyclonic wind shear indicates good outflow in association with the upper-level AC. Compared to the NCEP analysis, a smaller anti-cyclonic wind shear zone is simulated in the Bay of Bengal within this larger-scale anti-cyclonic wind shear zone. These results support the hypothetical mechanism suggested by *Anthes* [1982] that the occurrence of anti-cyclonic wind shear between 200 and 850 hPa wind might release dynamic instability for TC formation. This mechanism will be examined in more detail to understand during which stage the release of dynamic instability is crucial for the intensification of a pre-TC disturbance and/or a TC.

[15] Previous climate studies [e.g., *Joseph and Srinivasan*, 1999] in this region suggested that the upper-level divergent AC is associated with a Rossby wave and that deep convective heating is the energy source of the Rossby wave. To briefly illustrate the related moist processes during the intensification of Nargis, 2-day average precipitation from the model during April 27–29 (Figure 10a) is verified against NASA TRMM precipitation measurements (Figure 10b). Overall, the spatial distribution of the average precipitation is highly correlated with the location of the mesoscale vortex circulation. An average is used simply because precipitation fluctuates at timescales shorter than the large-scale circulation. In addition, the relatively coarse resolution and the stochastic nature of the individual convective cells make it very challenging to reproduce the small spatial and temporal variability of precipitation. Figures 10c and 10d show these fields in a 5° box near the vortex center for further comparison. In the model simulation, two local precipitation maxima appear on the east and west side of the simulated vortex center (Figure 10c). In comparison, the TRMM precipitation maximum occurs on the southwest side of the vortex center resolved in the NCEP analysis. The domain-averaged precipitation in the 5 (2) degree box is 59.7 (152.2) mm/day for the model and 61.8 (173.8) mm/day for TRMM. This indicates an underestimate of 3.4% (12.4%) in the 5° (2°) average precipitation by the model with a larger

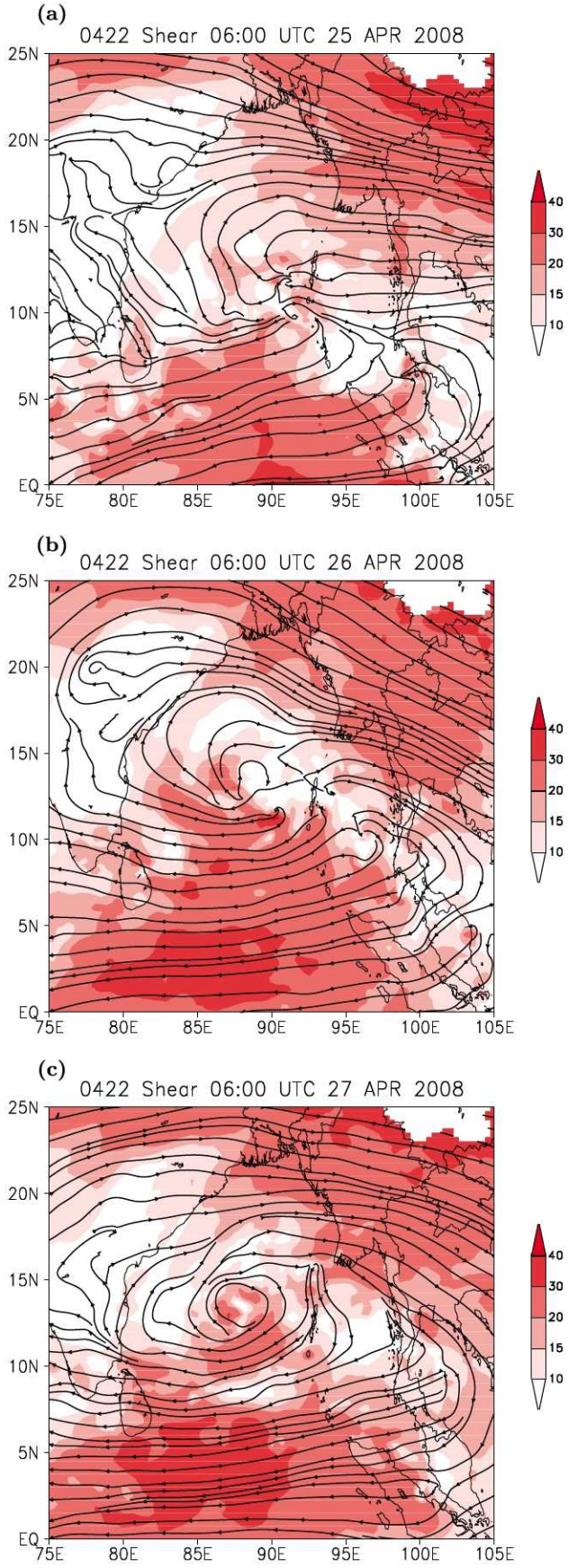

Figure 9. Streamlines of vertical wind shear between 200 and 850 hPa with magnitudes shaded in color after (a) 78, (b) 102, and (c) 126 h of integration, corresponding to 0600 UTC 25, 26, and 27 April 2008, respectively.

discrepancy for 2° average precipitation. This indicates the difficulty in automatically selecting a sample domain size, because an accurate assessment of the simulated precipitation associated with the vortex, including its location and scale, is important for quantitative comparison. Although there exists a displacement error due to the less accurate representation of Nargis in the model between day 5 and day 7, simulated precipitation from resolvable-scale condensation is on the same order as TRMM.

[16] Over its life time, Nargis' intensity was underestimated in the NCEP analyses (with a MSLP of about 1000 hPa). Therefore, QuikSCAT winds are used for further verification of the simulated near-eye wind speeds and vortex scale (e.g., radius of maximum winds). Due to the availability of QuikSCAT winds, three-hourly average 10m winds and QuickSCAT winds in a 2° × 2° box, ending at 12000 UTC April 28, are shown in Figures 11a and 11b, respectively. At this time, the best track indicates that Nargis was a category-1 storm with a maximum sustained wind speed of 65 knots (33.4 m/s). The simulated TC has a max 10-m wind speed of 30 m/s, which is slightly (3 m/s) weaker than the best track but (3 m/s) stronger than that in the QuikSCAT winds. The simulated vortex has a comparable scale but is more compact compared to QuikSCAT. To illustrate the simulated vertical structure of Nargis, a height-latitude cross section of zonal wind speeds (contour lines) and temperature anomalies (shaded) is plotted in Figure 12. This indicates the formation of a realistic elevated warm core from a weak disturbance (Figure 12a) to a TC at 1200 UTC 27 April (Figure 12b). It also clearly shows that the simulated storm intensified in association with the occurrence of upper-level outflow (Figure 12b) and anti-cyclonic vertical wind shear between 200 and 850 hPa (Figures 12b and 12c).

3.2. Experiments With a Different Resolution and Initial Conditions

[17] In this study, no attempt is made at determining the critical grid spacing that is required to accurately simulate the timing and location of Nargis' formation. Here, three additional runs at a 0.5° resolution are simply conducted and compared with the control run at 0.25° resolution. The goal is to improve our understanding of the model's physical processes with different moist schemes at different resolutions, which might lead to improvements in moist processes associated with cumulus parameterizations at coarse resolutions. The 4th experiment (D-E) has the same model configuration as the control run (with an explicit grid-scale condensation scheme) except for a coarser grid spacing. The 5th (D-CPS) and 6th (D-CPS6h) experiments include the usage of CPs with a relaxation time of 3 and 6 hours, respectively. Figure 13 shows time-longitude diagrams of 850-hPa zonal winds averaged over latitudes 5–10° for the CNTL (Figure 13a), D-E (Figure 13b), D-CPS (Figure 13c), and D-CPS6h (Figure 13d) cases, respectively. Besides the occurrence of the WWB at a later time, the westward movement of easterly winds at an earlier time is clearly

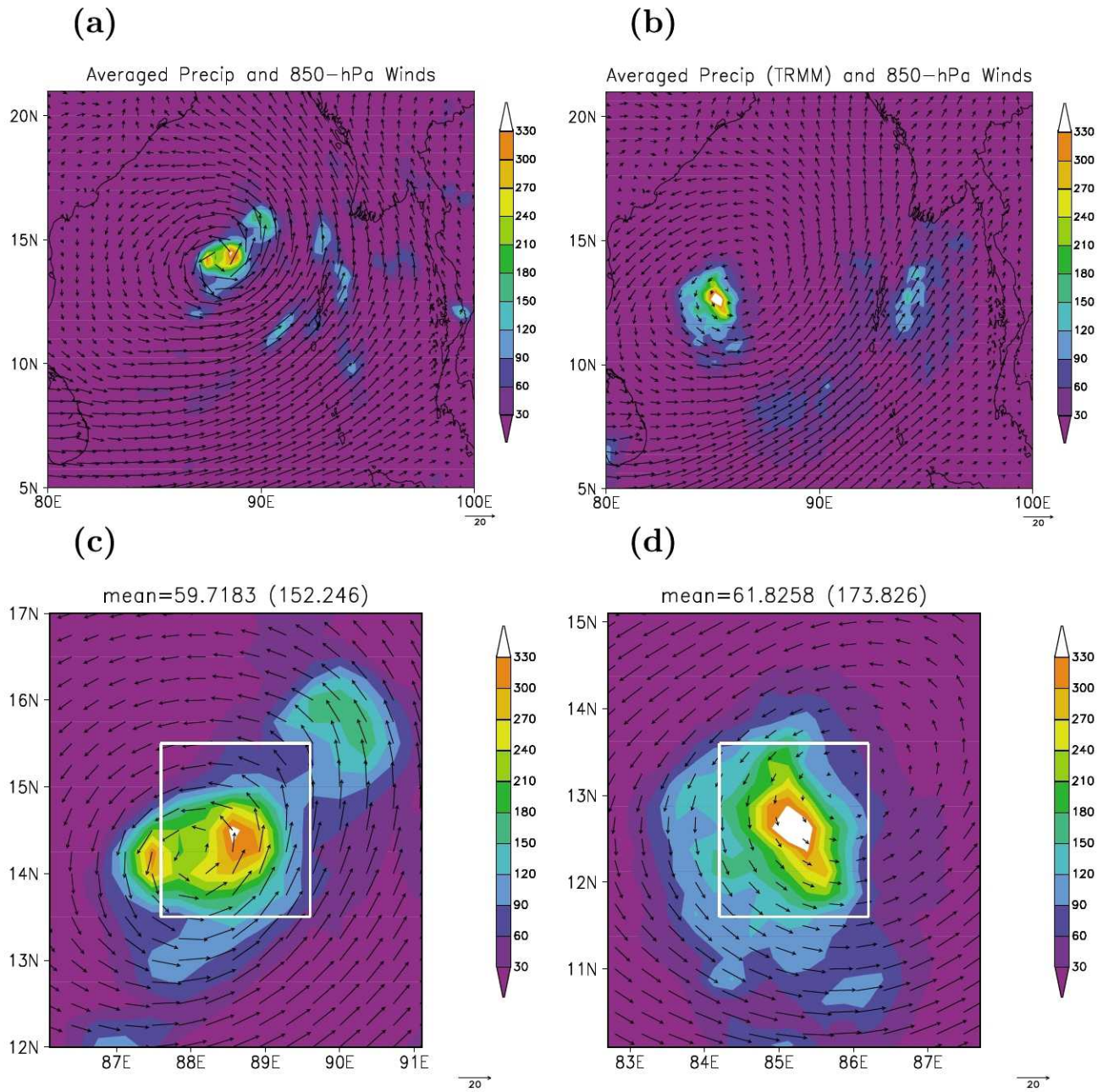

Figure 10. Averaged precipitation and wind vectors. (a) The 2-day average precipitation (shaded) and 850-hPa winds (vectors) from 0000 UTC April 27 (day 5) to 29 (day 7) and (b) NASA TRMM precipitation and NCEP analysis winds. (c, d) The same fields as Figures 10a and 10b, respectively, in a 5° box, centered at the maximum of precipitation near the vortex center.

shown in Figure 13a. As the easterly winds start interacting with the westerly winds on April 25, cyclonic wind shear appears along longitude 90°E. This shear contributes to the formation of a pre-TC mesoscale vortex at (9.5°N, 89.5°E) at 0000 UTC April 25. Except for the 0.5° experiment without CPs, the other 0.5° runs have similar patterns to the control run, but there are some differences (Figures 13c and 13d) in the location and timing for the interactions of the WWB and the easterly winds. In the 0.5° run with no CPs (Figure 13b), the maximum in the westerly winds shifts eastward for about 3 ~ 4 degrees, which is related to the inaccurate simulation of a pre-TC vortex discussed below. For the D-CPS and D-CPS6h cases, a pre-TC vortex appears at (10°N, 87.5°E) at 1200 UTC April 25 and at (7.5°N, 90°E) at 0600 UTC April 25, respectively. These differences in the location and timing of a mesoscale vortex are related to the variance in the simulations of the WWB and the easterly winds (i.e., large-scale flows). However, these cannot be precisely identified in the time-longitudes diagram of averaged zonal winds.

[18] As shown in Figure 14, these 0.5° runs are able to simulate the formation of a mesoscale vortex with a hurricane-scale intensity, showing the influence of the large-scale environmental flows. However, compared to the real

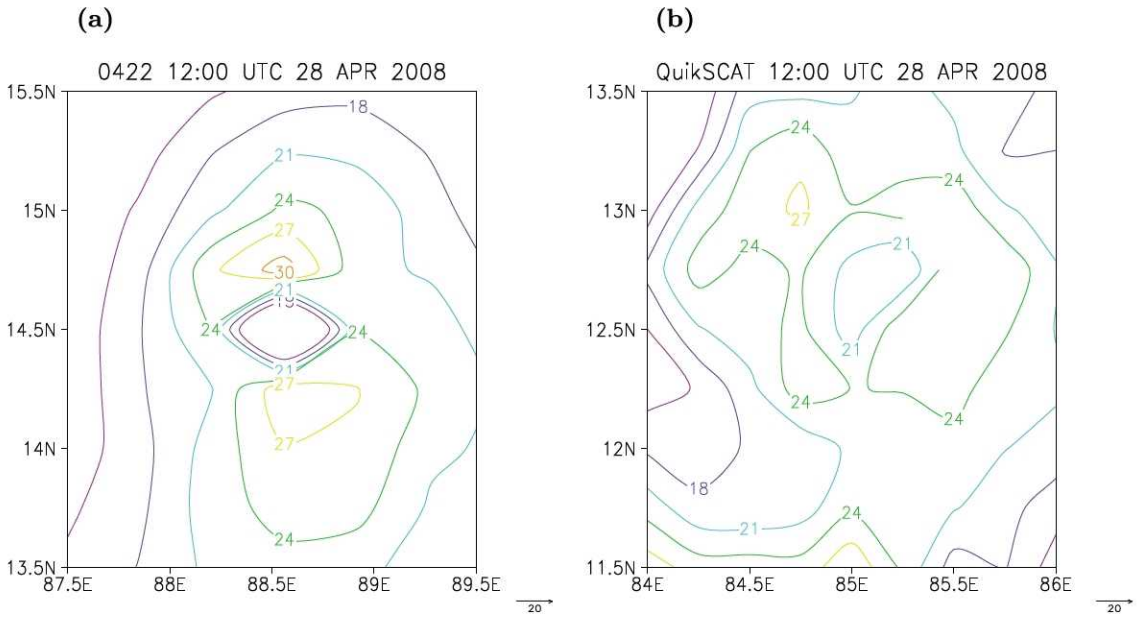

Figure 11. (a) Three-hourly averaged 10 m winds in a 2° box validated at 1200 UTC April 28 and (b) NASA QuikSCAT sea winds.

Nargis, the simulated vortex in case D-E without CPs has a large error in the location and path and thus cannot be identified as Nargis (Figure 14a). For practical purposes, an inaccurate prediction in movement is not very useful for providing a warning. This suggests that the resolved moist processes at this resolution and their feedback to the steering flows are not represented realistically. Interestingly, the simulated precipitation amount is slightly overestimated between day 5 and 7, because of less precipitation during the first 5 days of integration. In case D-CPS, which includes parameterized moist processes, the simulated TC has a displacement error (Figure 14b) comparable to the CNTL case; however, its intensity is weaker with a temporally- and spatially-averaged precipitation amount of 44 (114.6) mm/day for a 5 (2) degree box (Table 1). The overall spatial distribution of the average precipitation from these two runs (CNTL, D-CPS) is still well correlated with the location of the mesoscale vortex circulation. However, the difference in the predicted location of the vortex center suggests there are different feedback processes on the environment flows associated with the different moist processes from the different moist physics schemes. The results from cases D-E and D-CPS suggest the inclusion of parameterized moist processes could improve the initial formation and movement of Nargis in the 0.5° simulations. However, as convective processes are also partially resolved at the grid scale, hypothetically the interaction between the large-scale flows and the parameterized processes could possibly be relaxed further. To illustrate this, case D-CPS6h with a relaxation time of 6 hours is conducted. The D-CPS6h run shows improved simulations of Nargis' location and average intensity (Figure 14c) compared to D-CPS. The average temporal and spatial precipitation, shown in Table 1, is 64.0 (128.1) mm/day for a 5° (2°) box. Compared to the CNTL case, a large error in

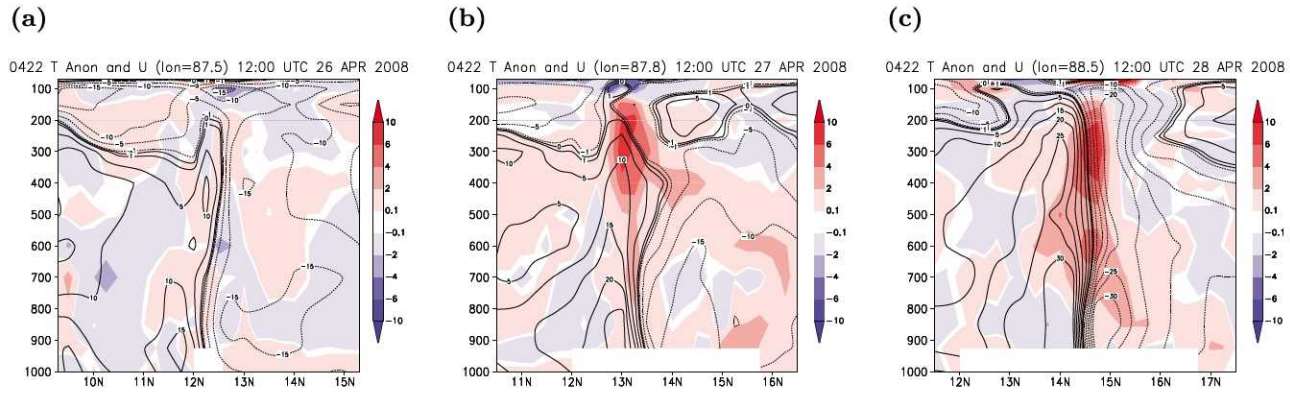

Figure 12. Vertical structure of zonal winds (m/s, contours) and temperature anomalies (°C, shaded) at 1200 UTC (a) 26, (b) 27 and (c) 28 April, showing the development of an elevated warm core during the enhancement of a pre-TC vortex (Figure 12a), the formation of TC Nargis (Figure 12b), and intensification of TC Nargis (Figure 12c).

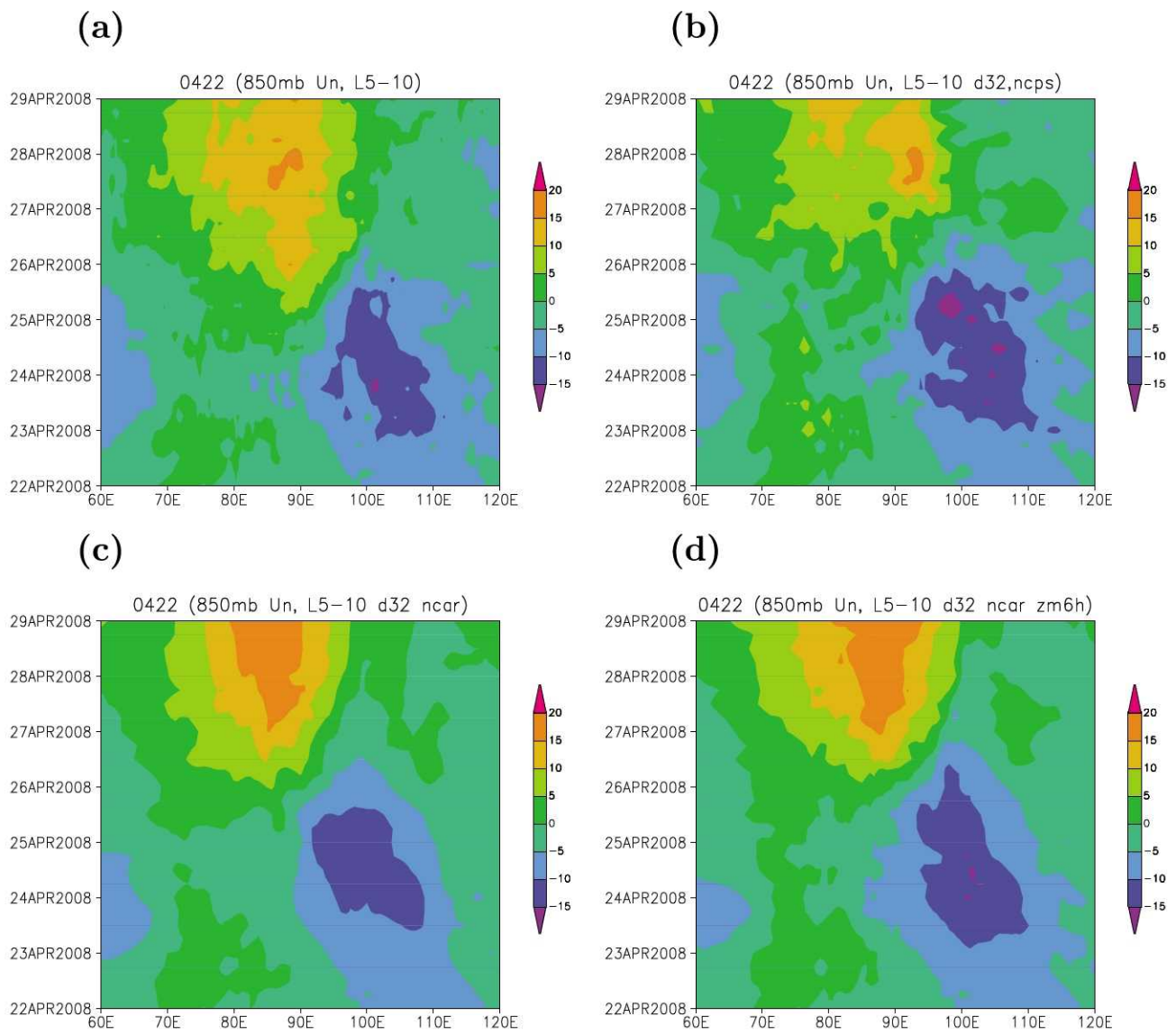

Figure 13. Time-longitude diagrams of 850 hPa zonal winds averaged over (5°N, 10°N). (a) Results from the control run at a 0.25 degree resolution. Numerical experiments at a 0.5° resolution (b) with an explicit grid-scale condensation scheme only, (c) with cumulus parameterizations (CPs) included, and (d) with CPs and a different relaxation time.

the 2° average precipitation in D-CPS6h, which is 26% less, indicates the sensitivity of the larger resolved scale to the coarser grid spacing. Thus, the results from these CNTL, D-E, D-CPS and D-CPS6h cases illustrate a positive impact on the simulation of moist processes and their interactions with environmental flows by increasing the resolution (from 0.5° to 0.25°). However, a systematic study is still desired.

[19] The dependence of multiscale simulations on different dynamic initial conditions is discussed in the following. Results from two additional 0.25° experiments (E-23 and E-24), which are initialized at 0000 UTC April 23 and 24 2008, are shown in Figures 15a–15c and 15d–15f, respectively. In Figure 15a (Figure 15d), the spatial distribution of MSLP during the first 6 (5) days of integration, ending at 0000 UTC April 29, qualitatively indicates the location of the initial formation of the simulated vortex and its subsequent movement. Overall, these are in good agreement with the observation. However, E-23 and E-24 predict the formation of Nargis at 0000 UTC April 26 and 1800 UTC April 25, respectively, which are about 36 and 42 hours earlier. The differences in the timing of the vortex formation from the three 0.25 degree runs may be partially related to a spin-up problem (in particular associated with precipitation processes), because only dynamics fields (winds, potential temperature, humidity) from NCEP analysis are used as the model initial conditions. Figures 15b and 15e show that the average precipitation and vortex circulations are correlated. The simulated storms are also slightly stronger than in the control run (Table 1). A closer look at the simulated 10m winds at 1200 UTC April 28 suggests the simulated max wind speed in case E-23 (Figure 15c) is about 3m/s stronger than that in the control but is closer to the best track. The simulated vortex center in E-24 is surprisingly close to that in E-23; its maximum wind speed is 3 m/s weaker. All three of

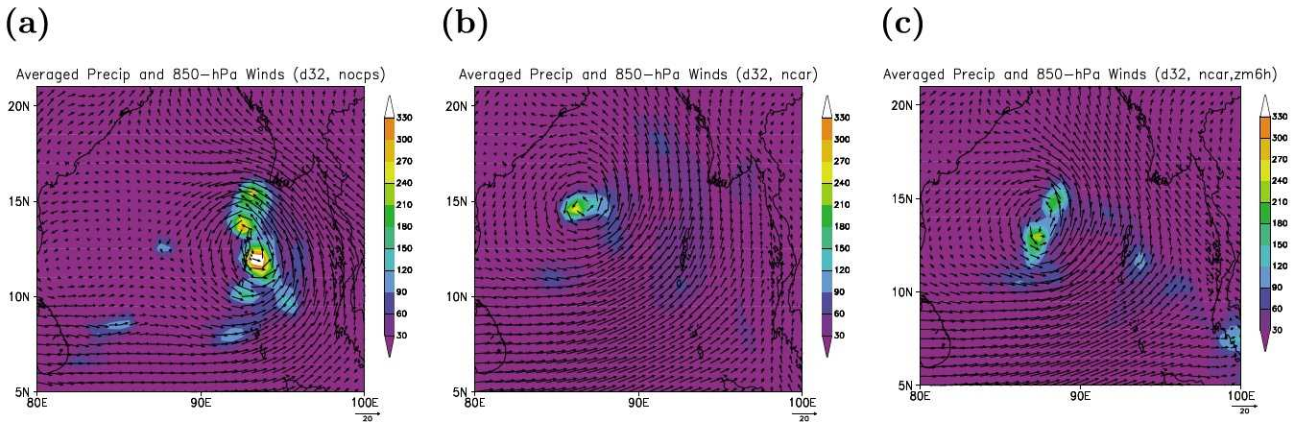

Figure 14. Numerical experiments at a 0.5° resolution (a) with an explicit grid-scale condensation scheme only, (b) with cumulus parameterizations (CPs) included, and (c) with CPs and a different relaxation time. Shown are averaged precipitation (shaded) and 850-hPa wind vectors averaged from 0000 UTC April 27 (day 5) to 29 (day 7).

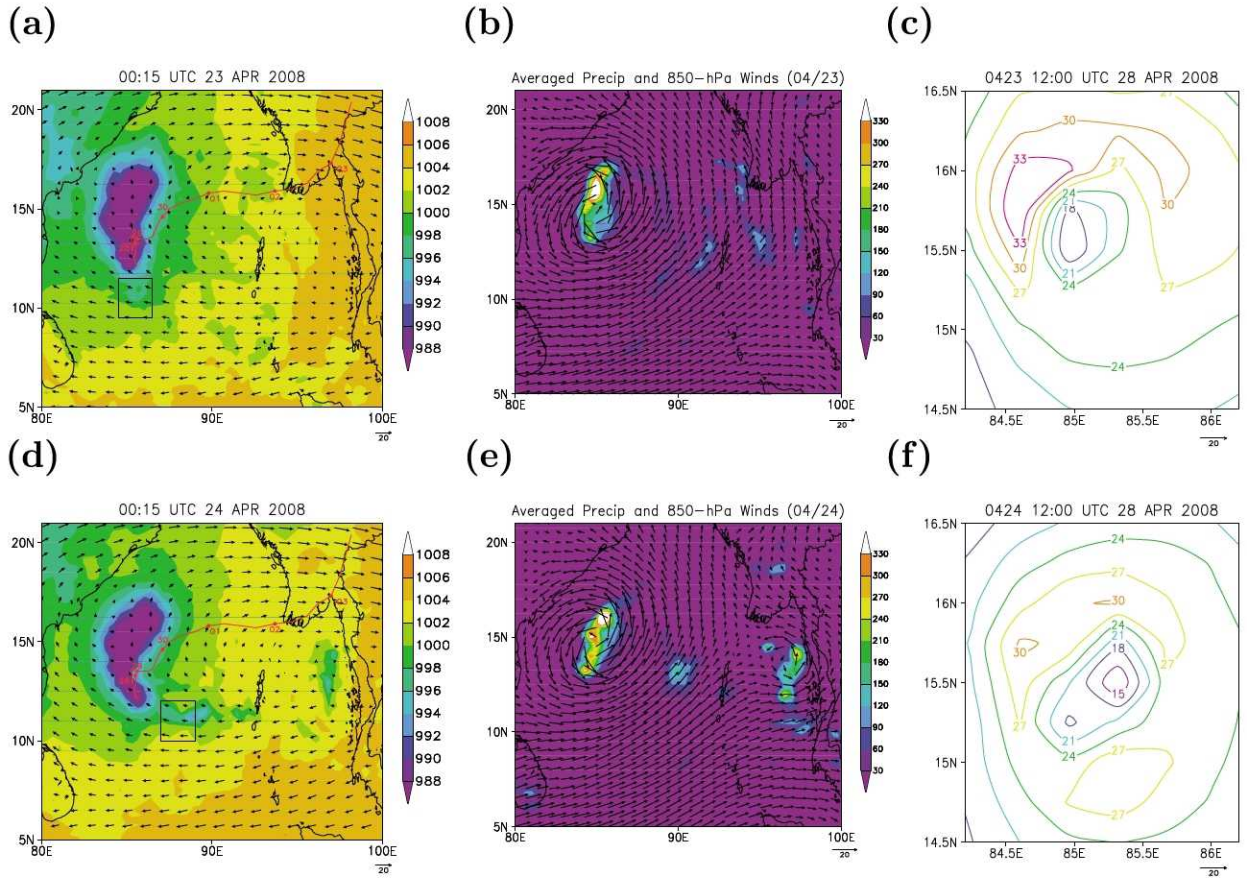

Figure 15. Experiments with dynamic initial conditions at (a, b, c) 0000 UTC April 23 and (d, e, f) 0000 UTC April 24. Figures 15a and 15d show spatial distribution of minimum SLP over the first 6 and 5 day integration period, respectively, ending at 0000 UTC April 29. Averaged 200-hPa winds are shown in vector. A 2 degree square box shows the initial location of the simulated Nargis at 0000 UTC April 26 in Figure 15a and 1800 UTC April 25 in Figure 15d. Figures 15b and 15e display precipitation and 850-hPa wind speeds averaged over the period of April 27–29. Figures 15c and 15f shows 10m winds, ending at 1200 UTC April 28, in a 2 degree box near the vortex center.

the 0.25 degree runs produce a comparable and realistic vortex scale (in terms of radius of max winds) as compared to the QuikSCAT winds at 1200 UTC April 28, 2008. Thus, although the model resolution (0.25 degree) is not yet sufficient to resolve small-scale convection, global simulations can still capture realistic TC formation with some degree of satisfaction. (By conducting shorter-term numerical experiments on a 0.15 degree unstaggered grid with a limited-area model, *Tory et al.* [2006a, 2006b] reached a similar conclusion that: TC formation can be predicted at a lead time of 24–36 hours without detailed simulations of small-scale convection.) This can be explained by the hierarchical multiscale interactions, namely, the modulation and feedback between larger-scale forcing and smaller-scale flows. (A parallel run on an aqua planet is also performed, showing the importance of land's mechanic and thermodynamic effects in simulating environmental circulations and in determining the location and timing of Nargis' formation and movement. This will be discussed in detail in a separate article.) These include the modulation of the formation and movement of a mesoscale vortex by (strong) environmental conditions such as the WWB and equatorial trough, and the subsequent modulation of convective processes by the mesoscale vortex.

[20] During its entire life cycle (27 April to 3 May), TC Nargis is not well resolved in the NCEP analyses (with a MSLP of about 1000 hPa). This is due in part to the sparse observations in this area, which makes it very challenging to predict Nargis' movement and intensification. However, it is encouraging that simulations with NCEP analyses from an earlier time prior to Nargis' formation (e.g., 22–24 April) show a great deal of promise in predicting Nargis' formation. This implies that not only are the characteristics of the large-scale flows represented realistically in NCEP analysis but so too are their potential impacts (e.g., modulation) on small-scale flows, which is vital to the model's ability to predict TC formation.

4. Concluding Remarks

[21] In this study, 7-day high-resolution (0.25°) global simulations of Tropical Cyclone Nargis (2008) are conducted with an explicit grid-scale condensation scheme to investigate the multiple processes and their scale interaction that lead to its formation with the aim of improving the lead time for TC genesis. Though Nargis' unusual movement within its short life cycle made it challenging to forecast, its formation (and the appearance of a pre-TC disturbance) is predicted five days in advance with position errors of 200 km. Nargis' rapid recurvature and intensification over the following two days is also simulated realistically except that the simulated propagation speed is too fast. High-resolution numerical experiments suggest the following processes and their hierarchical multiscale interactions lead to the formation of TC Nargis: a WWB moving northward, the interaction of its leading edge with easterly winds along its northern periphery, the generation of cyclonic shear, and the subsequent pre-TC mesoscale vortex. The simulations also showed that peaks in low-level convergence and the occurrence of WWBs were associated with the formation of a pre-TC vortex and the formation of Nargis. During this early stage, the monsoonal circulation (low-level cyclonic circulation and upper-level anti-cyclonic circulation) was enhanced, and anti-cyclonic wind shear developed between 200 and 850 hPa in association with good upper-level outflow. Both contributed favorably to the formation of Nargis. During the period of Nargis' intensification from April 27 to 29, the two-day average precipitation near the vortex circulation from the model simulation is in good agreement with that obtained from the NASA TRMM satellite, suggesting that the aggregate effects of the moist processes (e.g., surface fluxes and latent heating) are simulated reasonably well under strong environmental forcing. In summary, the favorable environmental conditions associated with the formation of TC Nargis were (1) a WWB and equatorial trough, (2) an enhanced monsoon circulation with a zero wind shear line, (3) good upper-level outflow with anti-cyclonic wind shear between 200 and 850 hPa, and (4) low-level moisture convergence.

[22] Though the individual contributions from the aforementioned processes are important, their relative role and their non-linear interaction over an entire TC life cycle make it a challenge to identify the critical processes. Further examination of their relative roles in TC genesis and intensification are desired with the aim of improving our understanding of the model's ability to simulate and investigate TC (hurricane) climate. The dependence of simulated multiscale flows on different grid spacing, CPs and initial conditions is illustrated with five additional 7-day experiments. For the Nargis case, the model at a 0.25° resolution with an explicit grid-scale condensation scheme is able to simulate these processes realistically, though variances in the timing and location are found in the simulations with different initial conditions. In contrast, the model at a 0.5° resolution with no CPs is not able to accurately simulate Nargis' formation and movement. With the inclusion of CPs, the coarser-resolution (0.5°) model is able to simulate these multiple processes with some degree of satisfaction. However, despite the differences in the timing and location of the simulated TCs, their intensity and scale are still weaker and larger than those in the high-resolution runs.

[23] As the high-resolution model shows the potential to improve genesis prediction at short-time (~5 day) scales, a comprehensive understanding of the strengths and weaknesses of the model's physical parameterizations (e.g., surface/boundary layer parameterizations) is required to improve overall model performance in simulating the above processes at different stages of a TC life cycle with the aim of understanding the model's performance in long-term integration. For example, between 120–148 hours into the simulations, the model vortex and its associated precipitation field have a displacement error of about 250–350 km. To reduce the error, future work should focus on improving the model's moist processes and on understanding how they feedback onto large-scale steering flows and mesoscale vortices. For developing storms in the western North Pacific, *Zehr* [1992] proposed a conceptual model that tropical cyclogenesis is associated with two distinct phases of enhanced convection, which is forced by external low-level wind convergence. While these Nargis simulations seem to support his findings, a systematic model evaluation with different cases is still desired. All of the aforementioned tasks are important, especially, for the accurate prediction of TC genesis. Through this, the detailed intensity

evolution of TC Nargis can be understood, and the false alarm rate for TC genesis in a global environment could be reduced. These tasks are the subject of a future study.

[24] An important implication of this study is that the predictability of mesoscale weather systems, which are not present initially, could be improved by a high-resolution global model that can properly represent the evolution of the initial larger-scale flow, its ability to modulate the smaller-scale flow, and the subsequent hierarchical scale interaction. As global models and data assimilation systems decrease their grid spacing to resolve mesoscale weather, a strategic plan on how to best evaluate the impact of large-scale initial conditions on the formation of mesoscale systems is desirable.

[25] **Acknowledgments.** We would like to thank three reviewers for their valuable suggestions, which have substantially improved the manuscript. We are grateful for support from the NASA Advanced Information System Technology (AIST) and Modeling Analysis Prediction (MAP) programs and the NSF Science and Technology Center for this study. We would like to thank Steve Lang and K.-S. Yeh for proofreading and reviewing this manuscript, B. Green for visualizations, K.-S. Kuo for the preparation of Figure 1, and H.-T. (Jenny) Wu, and Y. Jin (NRL) for valuable discussions. We also thank the NASA Advanced Supercomputing Division and NASA Center for Computational Sciences for computer time used in this research.

References

Aiyyer, A. R., and J. Molinari (2003), Evolution of mixed Rossby gravity waves in idealized MJO environments, *J. Atmos. Sci.*, *60*, 2837–2855.

Anthes, R. A. (1982), *Tropical Cyclones: Their Evolution, Structure, And Effects*, *Meteorol. Monogr.*, vol. 41, 208 pp., Am. Meteorol. Soc., Boston, Mass.

Atlas, R., O. Reale, B.-W. Shen, S.-J. Lin, J.-D. Chern, W. Putman, T. Lee, K.-S. Yeh, M. Bosilovich, and J. Radakovich (2005), Hurricane forecasting with the high-resolution NASA finite volume general circulation model, *Geophys. Res. Lett.*, *32*, L03807, doi:10.1029/2004GL021513.

Atlas, R., S.-J. Lin, B.-W. Shen, O. Reale, and K.-S. Yeh (2007), Improving hurricane prediction through innovative global modeling, in *Extending the Horizons: Advances in Computing, Optimization and Decision Technologies*, edited by E. Baker et al., pp. 1–14, Springer, New York.

Biswas, R., M. J. Aftosmis, C. Kiris, and B.-W. Shen (2007), Petascale computing: Impact on future NASA missions, in *Petascale Computing: Architectures and Algorithms*, edited by D. Bader, pp. 29–46, CRC Press, Boca Raton, Fla.

Briegel, L. M., and W. M. Frank (1997), Large-scale influences on tropical cyclogenesis in the western North Pacific, *J. Atmos. Sci.*, *125*, 1397–1413.

Charney, J. G., and A. Eliassen (1964), On the growth of the hurricane Depression, *J. Atmos. Sci.*, *21*, 68–75.

Dunkerton, T. J., M. T. Montgomery, and Z. Wang (2008), Tropical cyclogenesis in a tropical wave critical layer: Easterly waves, *Atmos. Chem. Phys. Discuss.*, *8*, 11,149–11,292.

Emanuel, K. A. (1986), An air-sea interaction theory for tropical cyclones, Part I., *J. Atmos. Sci.*, *43*, 585–604.

Ferreira, R. N., and W. H. Schubert (1996), Dynamical aspects of twin tropical cyclones associated with the Madden-Julian Oscillation, *J. Atmos. Sci.*, *53*, 929–945.

Gray, W. M. (1975), Tropical cyclone genesis, *Dep. of Atmos. Sci. Pap. 234*, 121 pp., Colo. State Univ., Ft. Collins.

Gray, W. M. (1979), Hurricanes: Their formation, structure and likely role in the tropical circulation, in *Meteorology Over the Tropical Oceans*, edited by D. B. Shaw, pp. 155–218, RMS, Bracknell, U. K.

Hack, J. J. (1994), Parameterization of moist convection in the NCAR CCM2, *J. Geophys. Res.*, *99*, 5551–5568.

Hendrick, E. A., M. T. Montgomery, and C. A. Davis (2004), The role of "vortical" hot towers in the formation of tropical cyclone Diana (1984), *J. Atmos. Sci.*, *61*, 1209–1232.

Holland, G. J., and P. Webster (2005), Scale interactions and tropical cyclone genesis: Why global models have skill, paper presented at 59th Interdepartmental Hurricane Conference, Univ. of N. Fla., Jacksonville.

Joseph, P. V., and J. Srinivasan (1999), Rossby waves in May and the Indian summer monsoon rainfall, *Tellus, Ser. A*, *51*, 854–864.

Kuo, H.-C., J.-H. Chen, R. T. Williams, and C.-P. Chang (2001), Rossby waves in zonally opposing mean flow: Behavior in Northwest Pacific Summer Monsoon, *J. Atmos. Sci.*, *58*, 1035–1050.

Lin, S.-J. (2004), A vertically Lagrangian finite-volume dynamical core for global models, *Mon. Weather Rev.*, *132*, 2293–2307.

Liu, W. T., W. Tang, and P. Polito (1998), NASA scatterometer provides global ocean-surface wind fields with more structures than numerical weather prediction, *Geophys. Res. Lett.*, *25*, 761–764.

Madden, R. A., and P. R. Julian (1971), Detection of a 40–50 day oscillation in the zonal wind in the tropical Pacific, *J. Atmos. Sci.*, *28*, 702–708.

Maloney, E. D., and D. L. Hartmann (2000a), Modulation of hurricane activity in the Gulf of Mexico by the Madden-Julian oscillation, *Science*, *287*, 2002–2004.

Maloney, E. D., and D. L. Hartmann (2000b), Modulation of eastern North Pacific hurricanes by the Madden-Julian oscillation, *J. Clim.*, *13*, 1451–1460.

McBride, J. L., and R. Zehr (1981), Observational analysis of tropical cyclone formation. Part II: Comparison of non-developing versus developing Systems, *J. Atmos. Sci.*, *38*, 1132–1150.

Moncrieff, M. W., M. A. Shapiro, J. M. Slingo, and F. Molteni (2007), Organized tropical convection and the global circulation: Collaborative research at the intersection of weather and climate, *WMO Bull.*, *56*(3), 1–9.

Montgomery, M. T., M. E. Nicholls, T. A. Cram, and A. Saunders (2006), A "vortical" hot tower route to tropical cyclogenesis, *J. Atmos. Sci.*, *63*, 355–386.

Ooyama, K. (1964), A dynamical model for the study of tropical cyclone Development, *Geofis. Int.*, *4*, 187–198.

Ritchie, E. A., and G. J. Holland (1997), Scale interactions during the formation of Typhoon Irving, *Mon. Weather Rev.*, *125*, 1377–1396.

Shen, B.-W., R. Atlas, O. Reale, S.-J Lin, J.-D. Chern, J. Chang, C. Henze, and J.-L. Li (2006a), Hurricane forecasts with a global mesoscale-resolving model: Preliminary results with Hurricane Katrina (2005), *Geophys. Res. Lett.*, *33*, L13813, doi:10.1029/2006GL026143.

Shen, B.-W., W.-K. Tao, R. Atlas, T. Lee, O. Reale, J.-D. Chern, S.-J. Lin, J. Chang, C. Henze, and J.-L. Li (2006b), Hurricane forecasts with a global mesoscale model on the NASA Columbia supercomputer, *Eos Trans. AGU*, *87*(52), Fall Meet. Suppl., Abstract A13E-0986. (Available at http://atmospheres.gsfc.nasa.gov/cloud_modeling/docs/2006_AGU_Fall_Poster.ppt)

Shen, B.-W., W.-K. Tao, R. Atlas, Y.-L. Lin, R. Reale, J.-D. Chern, C.-D. Peters-Lidard, and K.-S. Kuo (2007), Forecasts of tropical cyclogenesis with a global mesoscale model: Modulation of six tropical cyclones by the MJO in May 2002, paper presented at CMMAP Team Meeting, Colo. State Univ., Fort Collins. (Available at http://www.cmmap.org/research/docs/jul08/poster-shen2.pdf)

Simpson, J., E. Ritchie, G. J. Holland, J. Halverson, and S. Stewart (1997), Mesoscale interactions in tropical cyclones genesis, *Mon. Weather Rev.*, *125*, 2643–2660.

Sundqvist, H. (1988), Parameterization of condensation and associated clouds in models for weather prediction and general circulation simulation, in *Physically-Based Modeling and Simulation of Climate and Climatic Change*, vol. 1, edited by M. E. Schlesinger, pp. 433–461, Kluwer Acad., Norwell, Mass.

Tory, K. J., M. T. Montgomery, and N. E. Davidson (2006a), Prediction and diagnosis of tropical cyclone formation in an NWP system. Part I: The critical role of vortex enhancement in deep convection, *J. Atmos. Sci.*, *63*, 3077–3090.

Tory, K. J., M. T. Montgomery, N. E. Davidson, and J. D. Kepert (2006b), Prediction and diagnosis of tropical cyclone formation in an NWP system. Part II: A diagnosis of tropical cyclone Chris formation, *J. Atmos. Sci.*, *63*, 3091–3113.

Webster, P. J., and H.-R. Chang (1988), Equatorial energy accumulation and emanation regions: Impacts of a zonally varying basic state, *J. Atmos. Sci.*, *45*, 803–829.

Zehr, R. (1992), Tropical cyclogenesis in the western North Pacific, *NOAA Tech. Rep. NESDIS 61*, 181 pp., U. S. Dep. of Commer., Washington, D. C.

Zhang, G. J., and N. A. McFarlane (1995), Sensitivity of climate simulations to the parameterization of cumulus convection in the Canadian Climate Center general circulation model, *Atmos. Ocean*, *33*, 407–446.

R. Atlas, AOML, NOAA, Miami, FL 33149, USA.

W. K. Lau, B.-W. Shen, and W.-K. Tao, Laboratory for Atmospheres, Code 613, NASA Goddard Space Flight Center, Greenbelt, MD 20771, USA. (Bo-Wen.Shen-1@nasa.gov)